



Control of Dynamic Stall of an Airfoil by Using Synthetic Jet Technology

Jianjun Feng¹ · Guojun Zhu¹ · Yuan Lin¹ · Yunzhe Li² · Guangkuan Wu¹ · Jinling Lu¹

Received: 19 April 2020 / Accepted: 17 September 2020 / Published online: 6 October 2020
© King Fahd University of Petroleum & Minerals 2020

Abstract

In this paper, the dynamic stall characteristics of the S809 airfoil have been numerically predicted, and the flow under dynamic stall condition has been controlled by introducing synthetic jet for enhancing the airfoil aerodynamic performance. In addition, experimental results have been adopted to validate the obtained numerical ones. The results show that the oscillation of the airfoil can delay the occurring of stall, and the stall angle of attack is increased from 9.5° to 13.1°. The introduction of synthetic jet can improve the lift coefficient of airfoil under dynamic stall conditions: The mean lift coefficient in a period of oscillation has been increased by 33%, and the drag coefficient has been reduced by 39%. Moreover, the stall angle of attack is increased from 13.1° to 16.2°. Therefore, the airfoil performance under dynamic stall condition could be greatly improved by the introduction of synthetic jet technology.

Keywords S809 Airfoil · Dynamic stall · Synthetic jet · Flow control · Characteristic

List of Symbols

α	Angle of attack	f_2	Frequency of the synthetic jet
α_{mean}	Mean value of angle of attack	F_D	Drag force of the airfoil
α_{amp}	Fluctuating amplitude of angle of attack	Re	Reynolds number
c	Chord length of the airfoil	SJ	Synthetic jet
C_L	Lift coefficient	t	Time
C_D	Drag coefficient	T_1	Period of the angle of attack
F_L	Lift force of the airfoil	T_2	Period of the synthetic jet, $1/f_2$
f_1	Frequency of the airfoil oscillation	U_∞	Incoming flow velocity
		V_{jet}	Velocity of the synthetic jet
		y^+	Dimensionless wall distance
		ρ	Air density
		θ	Angle of the synthetic jet

✉ Jianjun Feng
jianjunfeng@xaut.edu.cn

✉ Guojun Zhu
zhuguojun@xaut.edu.cn

Yuan Lin
linyuan_199407@163.com

Yunzhe Li
li_yunzhe@zhefu.cn

Guangkuan Wu
wuguangkuan@xaut.edu.cn

Jinling Lu
jinling_lu@126.com

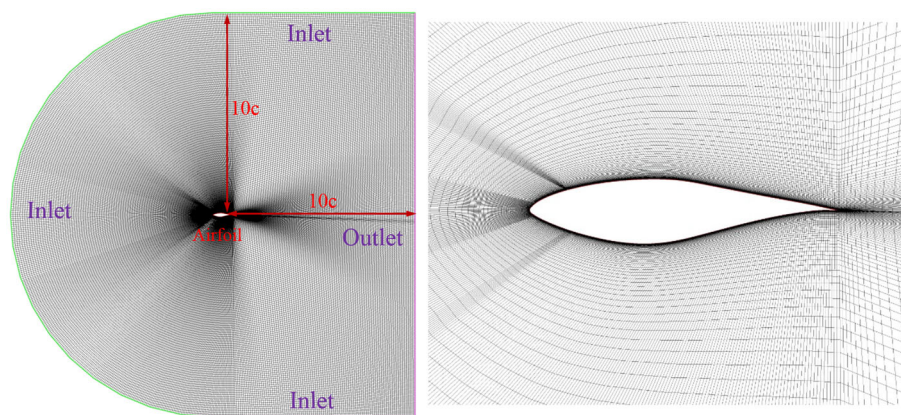
- 1 State Key Laboratory of Eco-Hydraulics in Northwest Arid Region of China, Xi'an University of Technology, Xi'an 710048, China
- 2 Fine Institute of Hydraulic Machinery, Zhejiang Fuchunjiang Hydropower Equipment Co., LTD., Hangzhou 311121, China

1 Introduction

For an airfoil, the lift-to-drag ratio increases gradually with angle of attack. However, when the angle of attack reaches a certain critical value, the reverse pressure gradient occurring will inevitably drive the flow separate from the airfoil surface, reducing the lift and increasing the drag. When the lift-to-drag ratio starts to decline due to the increasing extent of flow separation, the stall phenomenon happens [1]. The flow control technology is to intervene the flow by applying external forces or injection quality to the fluid, in order to improve the flow behavior and consequently to increase



Fig. 1 Computational model and partial mesh view



the lift, reduce the drag and eliminate or suppress the noise induced by the flow [2].

The synthetic jet (SJ) technology was initially developed by Smith and Glezer [3] and widely applied for active flow control, with the advantage of no requirement on additional energy input to the flow. The piezoelectric film of a SJ actuator is continuously vibrated to generate a periodic motion of blowing–sucking of air, producing a series of unsteady vortex pairs propagating downstream, and the boundary layer is therefore energized during the transportation of the fluid [3–5]. Zdenek and Vaclav [6] found that the jet vortices produced by the synthetic jet in small amplitude can last for a long time. If the amplitude is large, the speed of jet vortex breaking and merging will be much faster. Shaw et al. [7] developed an active flow control system on the F16 aircraft and tested it. Gilarranz and Rediniotis [8] have developed a compact synthetic jet which could be installed inside the NACA0015 airfoil. Qin et al. [9] applied the jet to a compressor airfoil. The result showed the maximum loss of the airfoil was reduced by 21.63%, and the pressure was increased by 5.6%. Gliarranz et al. [8, 10] experimentally applied a synthetic jet to control the NACA0015 airfoil, resulting in an increase in stall angle of attack from 12° to 18° . In addition, some researches have been conducted to examine the effects of SJ geometry and controlling parameters on airfoil characteristics, such as the work conducted by Zhao et al. [11] for the airfoil OA212 and by Feng et al. [12] for the S809 airfoil.

For an airfoil, the dynamic stall can be controlled by the oscillation of the airfoil or the variation of angle of attack with time, in which the aerodynamic characteristics of the airfoil will present a relatively obvious nonlinear hysteresis phenomenon [13]. McCroskey and Pucci [14] summarized four types of dynamic stall from no stall to deep stall, and the deep dynamic stall is characterized by large extent of flow separations and vortices on the airfoil [15, 16]. Some researches have been conducted for controlling dynamic

stall. For example, Sahin et al. [17] numerically examined the effect of deformed leading edge on airfoil dynamic stall. Modi [18] studied the effects of rotating cylinder on dynamic stall behavior of an airfoil by experimental methods, observing that the rotating cylinder would increase significantly the lift. However, applying the synthetic jet technology to control dynamic stall is relatively scarce, which therefore needs to be examined.

In this paper, numerical simulations have been conducted for the S809 airfoil under dynamic stall condition at $Re = 1 \times 10^6$. The obtained numerical results are compared with experiments, with more attention paid on aerodynamic characteristics under dynamic stall. Furthermore, the synthetic jet technology is applied to control the dynamic stall of the airfoil, and the control mechanism of the dynamic stall and its influence on airfoil aerodynamic performance are investigated in detail.

2 Numerical Procedures

The S809 airfoil [19] is selected for investigation, with a C-typed computational domain embracing the airfoil schematically illustrated in Fig. 1, and $c = 0.6$ m is the airfoil chord length. The mesh for the computational domain is created by using ANSYS ICEM-CFD [20], with the mesh around the airfoil demonstrated in an enlarged view.

In this paper, the dynamic stall is realized by the sinusoidal pitching motion of the airfoil, which is equivalent to the sinusoidal variation of the angle of attack (α) of the incoming flow, as expressed in Eq. (1):

$$\alpha = \alpha_{\text{mean}} + \alpha_{\text{amp}} \sin(2\pi f_1 t) \quad (1)$$

Referring to the settings for the S809 airfoil in the experiment conducted by Ramsay et al. [21] and numerical modeling performed by Gharali and Johnson [13], the param-

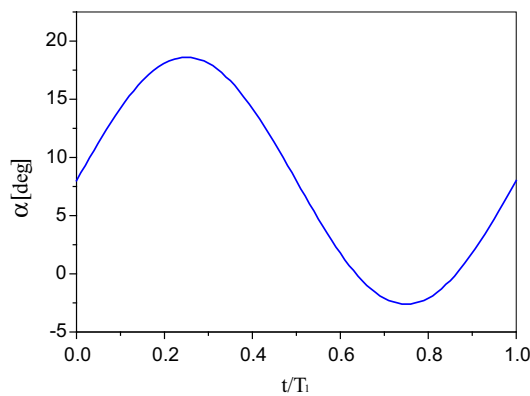


Fig. 2 Variation of angle of attack with time

eters regarding angle of attack for numerical simulations are defined: $\alpha_{\text{mean}} = 8^\circ$, $\alpha_{\text{amp}} = 10.6^\circ$ and $f_1 = 0.378$ Hz. Figure 2 shows the variation of angle of attack with time during one period T_1 .

For the computational domain demonstrated in Fig. 1, both the inlet and outlet boundary conditions are consistent with those for experiments [21]. A velocity of $U_\infty = 27.38$ m/s corresponding to $\text{Re} = 1 \times 10^6$ is specified at the inlet, and the flow direction varies with time according to Eq. (1). For the outlet, a constant pressure is defined. The wall is simulated by no-slip condition. Furthermore, the $k - \omega$ SST model is chosen for simulating the turbulent flow [22]. The time-step of simulations is set to 0.026478 s, which corresponds to 1/100 of the period of attack angle variation (T_1). In each time step, the convergence criterion is set for the average residuals below 10^{-6} .

Figure 3 is the layout of the SJ arrangement for the airfoil. According to Ref [12, 23], the hole for SJ is positioned on the airfoil upper side, with a width of 1% c and 12% c away from the airfoil leading edge. The jet frequency is $f_2 = 75$ Hz. The angle between the surface tangential direction and the jet flow direction, denoted as the jet angle θ , is set to 45° . In addition, the jet velocity V_{jet} defined in Eq. (2) varies periodically with time in the form of sine function during a jet period T_2 which can be calculated by $1/f_2$.

$$V_{\text{jet}} = 3V_\infty \sin(2\pi f_2 t) \tag{2}$$

The lift and drag coefficients, denoted by C_L and C_D , are calculated below [19]:

$$C_L = \frac{F_L}{0.5\rho c U_\infty^2} \tag{3}$$

$$C_D = \frac{F_D}{0.5\rho c U_\infty^2} \tag{4}$$

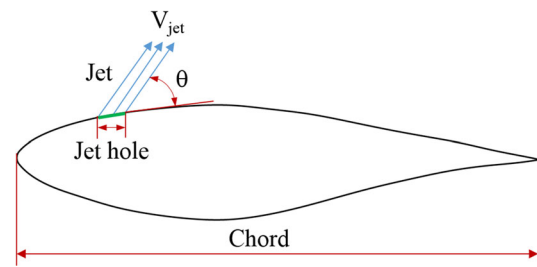


Fig. 3 Layout of synthetic jet on airfoil

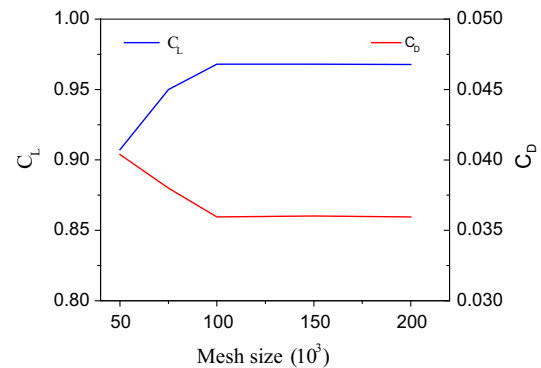


Fig. 4 Characteristic at different mesh size

where F_L is and F_D are the lift and drag forces of the airfoil, respectively; ρ is the density of air.

3 Results

3.1 Without SJ Control

Figure 4 presents the airfoil lift and drag coefficients near critical static stall condition ($\alpha = 11^\circ$) for different mesh sizes. It is found that when the mesh size exceeds 100,000, further increase in mesh size does not cause evident change on either the lift or drag coefficients. Meanwhile, during the mesh generation, the position of the first mesh node to the wall is well controlled to ensure y^+ below 10, which is suitable for the accurate solution of boundary layer for the selected turbulence model.

Figure 5 presents the comparison of airfoil characteristics at static condition (in which the angle of attack is independent of time) between CFD results and experimental ones. The experiments are conducted in a closed-throat, single-return, atmospheric wind tunnel, with a test section of 1.8 m in width and 1.25 m in height [19]. Although some differences exist for deep stall conditions with higher angles of attack, both the lift coefficient C_L and drag coefficient C_D predicted by CFD

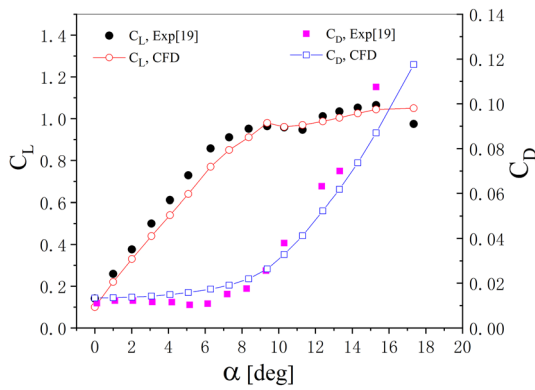


Fig. 5 C_L and C_D at static conditions

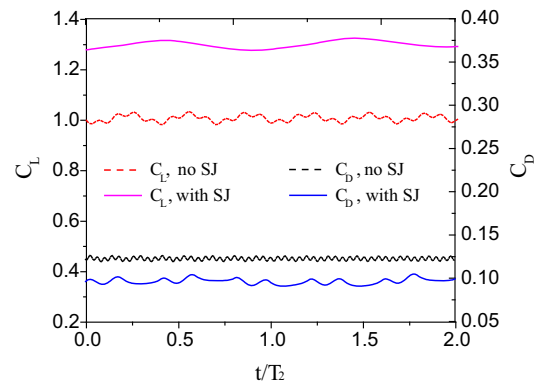
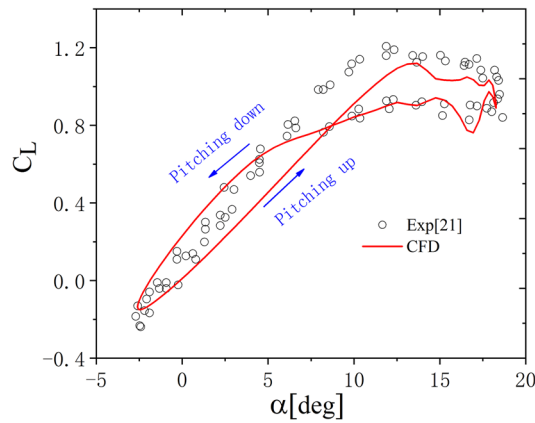
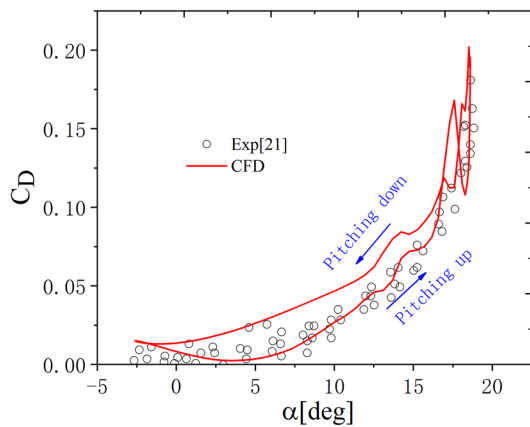


Fig. 7 Effect of SJ on static stall, $\alpha = 19^\circ$



(a) Lift coefficient

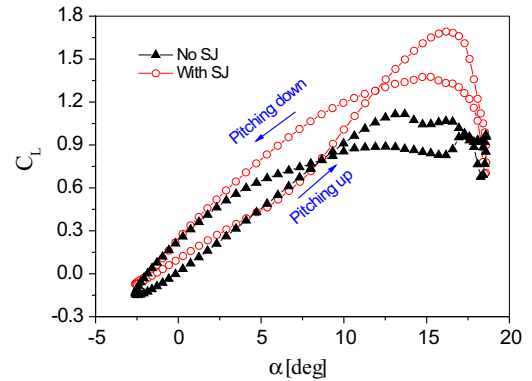


(b) Drag coefficient

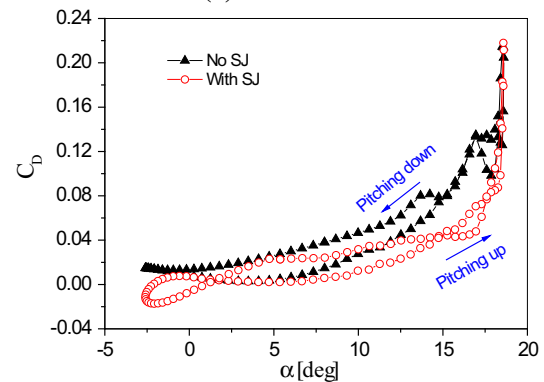
Fig. 6 Lift and drag coefficients during one oscillation period

show good agreement with experimental ones. Therefore, the applied numerical method has been validated.

Figure 6 plots the curves of C_D and C_L in one oscillation period obtained by CFD, which are compared with experimental results obtained in a subsonic wind tunnel. During the experiment, the oscillation of the S809 airfoil is realized by the motion of a cam driven by a motor, producing the



(a) Lift coefficient

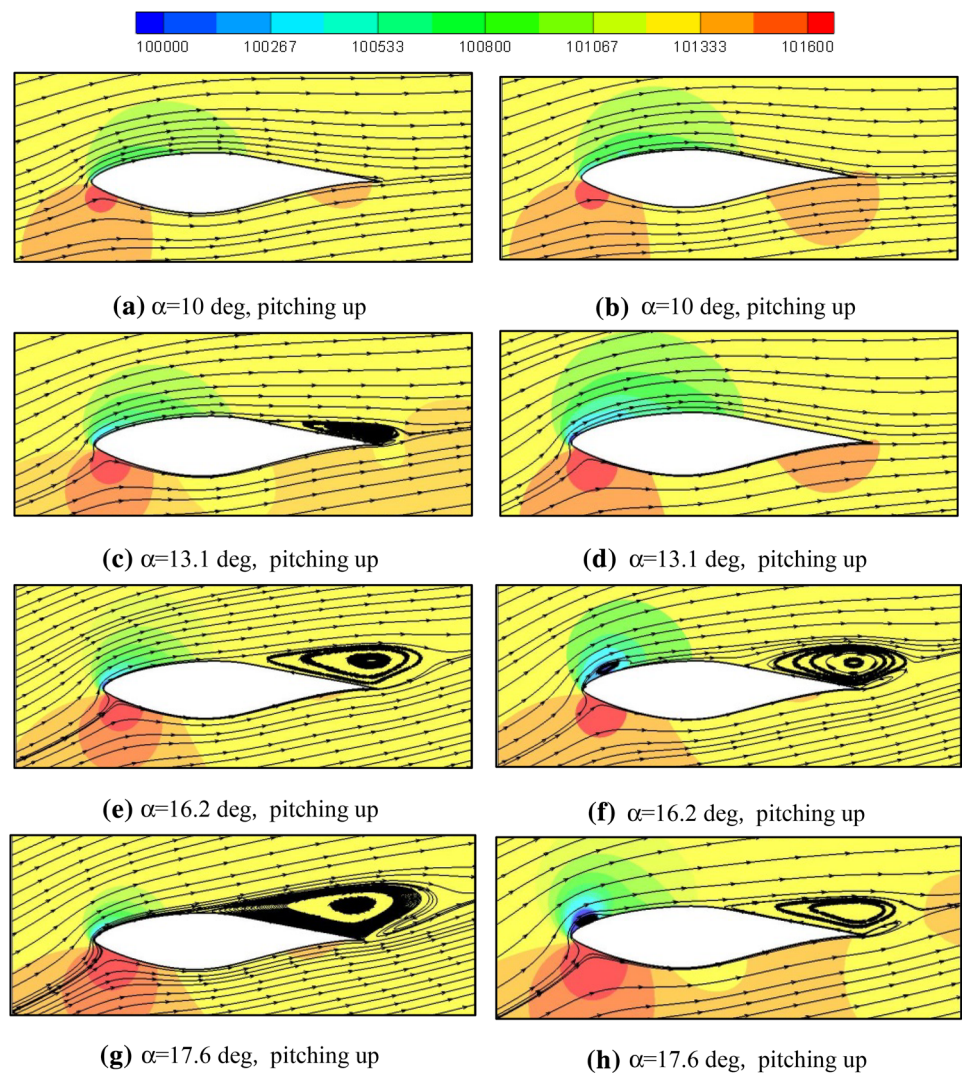


(b) Drag coefficient

Fig. 8 Comparison of airfoil performance

type and amplitude of the wave form required [21]. Although some differences can be observed for high angles of attack, the results from CFD and experiments show quite similar behavior. During one oscillating period, the angle of attack is increased first from 8° to 18.6° , then decreased from 18.6° to -2.6° , and again increased from -2.6° to 8° . For simplicity, the process during which the angle of attack keeps increasing from the minimum to maximum is named as pitching up process. Conversely, the process during which the angle of attack keeps decreasing is named as pitching down process. In the process of pitching up, the increase in angle of attack drives

Fig. 9 Comparison of flow structures during pitching up process: no SJ (left) and with SJ (right)



C_L to increase gradually. C_L starts to decline at the angle of attack of approximately 13.1° , indicating that the airfoil begins to stall and C_D rises rapidly with further increase in angle of attack. As the angle of attack declines from the maximum, C_L exhibits fluctuating behavior due to the unsteady stall. It is found that for the same angle of attack between the pitching up and down processes, the value of C_L is apparently different. C_L in the pitching up process is higher than that in the pitching down process when the angle of attack is higher than about 9° , and this phenomenon changes to the opposite direction when the angle of attack is lower than 9° . This hysteresis phenomenon occurring in the curves of C_L and C_D is caused by the dynamic stall of the airfoil.

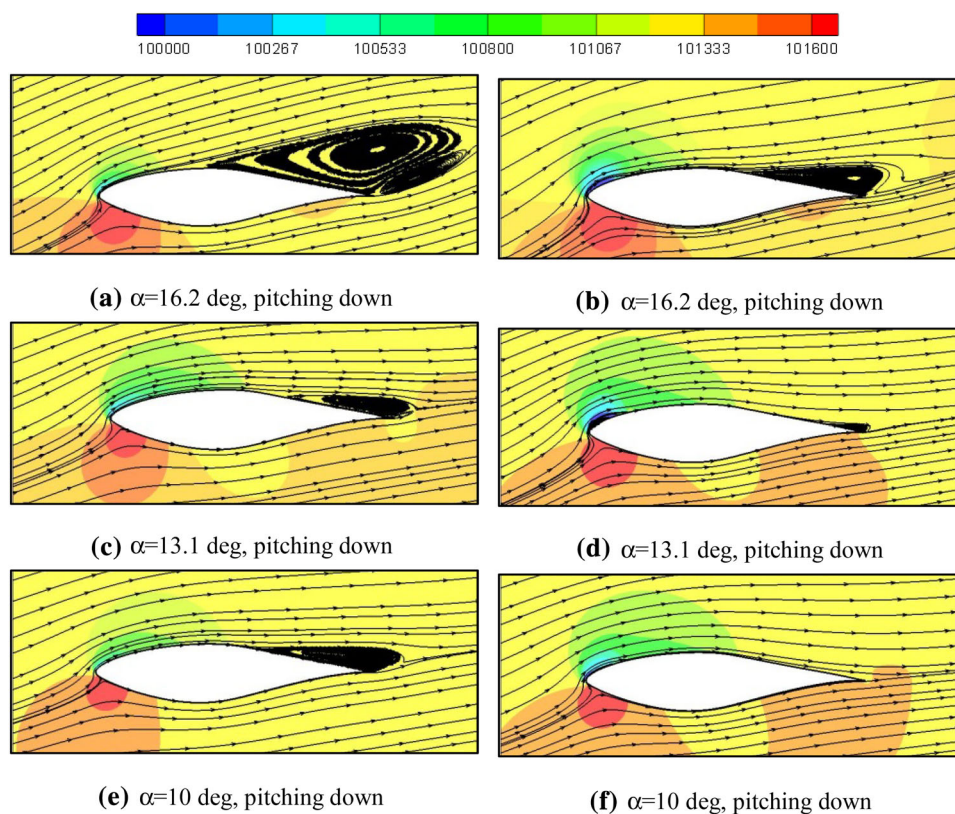
In addition, by comparing the curves of C_L in Figs. 5 and 6 between static stall and dynamic stall conditions, it is found that the angle of attack is 9.5° at static stall and 13.1° at dynamic stall, and the maximum values of C_L are 1.09 and 1.2, respectively. This shows that the oscillation of the airfoil delays the stall occurring and increases the peak value

of C_L , which is consistent with the conclusion reported by Tong [24].

3.2 With SJ Control

Prior to performing dynamic stall control to the airfoil, a static deep stall ($\alpha = 19^\circ$) is selected for adopting the SJ control, with the specific parameters mentioned above. Figure 7 presents the comparison of the dynamic performance of the airfoil before and after adding the SJ. It can be seen observed that in a SJ period (T_2), whether during the suction or blowing stage, the effect on enhancing aerodynamic characteristics is very evident. The lift coefficient C_L has been remarkably increased by the SJ, from the average of the fluctuating values in one period of approximately 1.0 to 1.3. Moreover, the drag coefficient C_D is also decreased by the SJ, from an average of approximately 0.125 to 0.1. Therefore, the application of SJ in static stall control has been validated.

Fig. 10 Comparison of flow structures during pitching down process: no SJ (left) and with SJ (right)



The variation of lift coefficient C_L with angle of attack during one oscillation period is illustrated in Fig. 8 for the S809 airfoil under dynamic stall condition. During the process of pitching up from 8° to 18.6° (Fig. 8a), C_L is greatly increased and the peak value is increased from 1.2 for to 1.69 by the introduction of SJ. Additionally, the stall angle of attack is also increased from 13.1° to 16.2° by the SJ. Similarly, during the process of pitching down from 18.6° to -2.6° , the SJ also significantly raises C_L at large angles of attack compared with no SJ. During the process of pitching up with the angle of attack ranging from -2.6° to 8° , C_L is basically unchanged. Therefore, when the angle of attack is greater than 8° , C_L with SJ is greater than that of no SJ, while when the angle of attack is smaller than 8° , the SJ has little effect on C_L . The average value of C_L is 0.568 in one oscillation period for the case without SJ, while 0.757 for the case with SJ. Therefore, the average C_L has been significantly augmented by 33% by the SJ control. Moreover, it is found from Fig. 8b that C_D is reduced in almost the entire range of angle of attack after the introduction of the synthetic jet. The average C_D has declined from 0.0536 to 0.0328, with a reduction rate of 39%, indicating the effectiveness of the airfoil stall control.

Figures 9 and 10 present the comparison of the streamlines before and after adding the SJ control, with contours colored by pressure. The streamlines in the left column are for the airfoil without SJ control, and the ones in the right

column are for the case with SJ control. For the case without SJ control, it can be observed that during the pitching up process, the flow near the trailing edge begins to separate from the upper surface caused by the large reverse pressure gradient at the angle of attack of 13.1° (Fig. 9c). This separation does not disappear at the angle of attack of 10° during the pitching down process (Fig. 10e), which has not been found at the same angle of attack for the pitching up process (Fig. 9a). This special behavior has resulted in different dynamic characteristics of the airfoil between the pitching up and down processes. As a result, a hysteresis phenomenon occurs in the characteristic curve of C_L and C_D shown in Fig. 8. Similar conclusion can be drawn for the case with SJ control. Furthermore, the controlling effect of the SJ is quite clear by comparing the streamlines. For example, the separation at $\alpha = 13.1^\circ$ without SJ has been removed totally by the SJ, both in the pitching up and pitching down processes (Figs. 9d and 10d).

4 Conclusion

In this paper, numerical simulations of dynamic stall for the S809 airfoil at a high Reynolds number of $Re = 10^6$ have been carried out, and the synthetic jet technology has been introduced to the airfoil for improving aerodynamic performance. The results show that the oscillation of the airfoil

can delay occurring of the stall. Compared with static condition, the stall angle of attack has been increased from 9.5° to 13.1° , and the maximum value of lift coefficient is increased from 1.09 to 1.2. Furthermore, the introduction of synthetic jet has improved the lift coefficient of airfoil under dynamic stall conditions: The average lift coefficient in a period of oscillation has been increased by 33%, the drag coefficient has been reduced by 39%, and the stall angle of attack has been increased from 13.1° to 16.2° as well. The comparison in detailed flow structure reveals that the flow structure has been improved by the synthetic jet. Consequently, the airfoil performance under dynamic stall condition has been greatly improved by the introduction of synthetic jet technology.

Author's Contribution J.F. guided the simulations and data analyses; Z.G. analyzed the data; L.Y. and L.Y. created the model and performed the simulations; W.G. and L.J. provided technical guidelines and scientific discussion. All authors have reviewed and agreed to publish the manuscript.

Funding This research was supported by the National Key R&D Program of China (2018YFB1501900), the National Natural Science Foundation of China (Grant Nos. 51909212 and 51879216), Natural Science Basic Research Plan in Shaanxi Province of China (No. 2019JQ-044) and Scientific Research Plan Projects of Shaanxi Provincial Department of Education (No. 19JK0570).

Compliance with Ethical Standards

Conflict of interest The authors declare that they have no conflict of interest.

References

- Moss, N.J.: Measurements of airfoil unsteady stall properties with acoustic flow control. *J. Sound Vib.* **65**, 505–520 (1979)
- Wang, L.: Flow characteristics of dual synthetic jets actuator and its application on an airfoil separate flow control. Doctoral dissertation, National University of Defense Science and technology (2009)
- Smith, B.L.; Glezer, A.: The formation and evolution of synthetic jets. *Phys. Fluids* **10**, 2281–2297 (1998)
- Luo, Z.B.; Xia, Z.X.; Deng, X.; et al.: Research progress of dual synthetic jets and its flow control technology. *Acta Aerodyn. Sin.* **35**, 252–264 (2017)
- You, D.; Moin, P.: Active control of flow separation over an airfoil using synthetic jets. *J. Fluids Struct.* **24**, 1349–1357 (2008)
- Zdenek, T.; Vaclav, T.: Annular synthetic jet used for impinging flow mass transfer. *Int. J. Heat Mass Transf.* **46**, 3291–3297 (2003)
- Shaw, L.; Smith, B.; Saddoughi, S.: Full scale flight demonstration of active flow control of a pod wake. AIAA 2006-3183 (2006)
- Gilarranz, J.L.; Rediniotis, O.K.: Compact, high-power synthetic jet actuators for flow separation control. AIAA Paper 2001-0737, (2001)
- Qin, Y.; Song, Y.P.; Wang, R.Y.; et al.: Flow separation control on a highly loaded compressor cascade using endwall synthetic jets. *J. Aerosp. Eng.* **232**, 2059–2075 (2017)
- Gilarranz, J.L.; Traub, L.W.; Rediniotis, O.K.: A new class of synthetic jet actuators, part II application to flow separation control. *J. Fluids Eng.* **127**, 377–387 (2005)
- Zhao, Q.J.; Ma, Y.Y.; Zhao, G.Q.: Parametric analyses on dynamic stall control of rotor airfoil via synthetic jet. *Chin. J. Aeronaut.* **30**, 1818–1834 (2017)
- Feng, J.J.; Lin, Y.; Zhu, G.G.; et al.: Effect of synthetic jet parameters on flow control of an aerofoil at high Reynolds number. *Indian Acad. Sci. Sadhana* **44**, 190 (2019)
- Gharali, K.; Johnson, D.A.: Numerical modeling of an S809 airfoil under dynamic stall, erosion and high reduced frequencies. *Appl. Energy* **93**, 45–52 (2012)
- Mc Croskey, W.J.; Pucci, S.L.: Viscous–inviscid interaction on oscillating airfoils in subsonic flow. *AIAA J.* **20**, 167–174 (1982)
- Mc Croskey, W.; Mc Alister, K.; Carr, L.: Dynamic stall on advanced airfoil sections. *J. Am. Helicopter Soc.* **26**, 40–50 (1981)
- Beddoes, T.: A qualitative discussion of dynamic stall. AGARD Rept. R-679 (1980)
- Sahin, M.; Sankar, L.N.; Chandrasekhara, M.S.; et al.: Dynamic stall alleviation using a deformable leading edge concept—a numerical study. *J. Aircraft* **40**, 77–85 (2003)
- Modi, V.J.: Moving surface boundary-layer control: a review. *J. Fluids Struct.* **11**, 627–663 (1997)
- Somers D.: Design and experimental results for the S809 airfoil NREL/SR-440-6918. Technical Report, NREL (1997)
- ANSYS ICEM CFD, Help System, Release 18.0, Ansys Inc., (2016)
- Ramsay, R.; Homan, M.; Gregorek, G.: Effects of grit roughness and pitch oscillation on the S809 airfoil. NREL/TP-442-7817. Technical Report, NREL (1995)
- Menter, F.R.: Two-equation eddy viscosity turbulence models for engineering applications. *AIAA J.* **32**, 1598–1605 (1994)
- Zhang, P.F.; Wang, J.J.: Numerical simulation on flow control of stalled NACA0015 airfoil with synthetic jet actuator in recirculation region. *J. Beijing Univ. Aeronaut. Astronaut.* **34**, 443–446 (2008)
- Tong, B.G.: *Unsteady Flow and Vortex Motion*. National Defense Industry Press, Beijing (1993)